University of Baghdad
College of Engineering
JOURNAL OF ENGINEERING

Journal of Engineering
journal homepage: www.jcoeng.edu.iq
Volume 32 Number 3 March 2026

Assessing Reservoir Heterogeneity through Integrated Petrophysical and Geological Modeling: Case Study of the Yamama Reservoir, Ratawi Field, Southern Iraq

Abdulrahman N. Al-Ansari[1,2,*], **Ayad A. Abdulrazaq**[1], **Dahlia A. Al-Obaidi**[1]

[1] Department of Petroleum Engineering, College of Engineering, University of Baghdad, Baghdad, Iraq
[2] Basrah Oil Company, Basrah, Iraq

ABSTRACT

Constructing a geologically realistic reservoir model and accurately evaluating petrophysical properties are critical components for effective reservoir management. Such efforts enable reliable assessment of hydrocarbon potential and support predictive development scenarios through numerical simulations. This study aims to characterize the Yamama carbonate reservoir in the Ratawi Field, southern Iraq, and to build a static geological model as a foundation for future dynamic simulation. Comprehensive well data, including wireline logs, core analysis, and geological reports, were integrated to interpret petrophysical parameters such as shale volume, effective porosity, and water saturation. Additionally, facies classification was performed using cluster analysis to define lithological variability across the reservoir. A structural framework was established based on contour maps and well tops, followed by 3D property modeling using geostatistical techniques. Experimental variogram models were constructed for each facies and zone to enhance distribution accuracy. The Yamama Formation was confirmed -consistent with previous studies- to consist of five vertical units, three reservoir-bearing (YA, YB, YC) and two barriers (C1, C2). However, this study uniquely establishes an evaluation framework using data from eight wells penetrating the formation, unlike earlier studies constrained by limited wells. Among these units, YB demonstrated the most favorable properties, accounting for approximately 63% of the estimated 1800 MMSTB OOIP, consistent with operator reports. Overall, reservoir quality improves northwestward and declines eastward, with moderate characteristics in the southern sector.

Keywords: Reservoir characterization, Geological modeling, Carbonate reservoir, Geostatistical analysis, Cluster analysis.

1. INTRODUCTION

Reservoir characterization relies fundamentally on interpreting well logs and core data, complemented by seismic inputs, to build geological models that represent reservoir

*Corresponding author
Peer review under the responsibility of University of Baghdad.
https://doi.org/10.31026/j.eng.2026.03.06

Article received: 05/10/2025
Article revised: 15/01/2026
Article accepted: 29/01/2026
Article published: 01/03/2026

geometry and dimensions. These models also illustrate the distribution of lithofacies and petrophysical properties, offering insight into storage capacity, fluid volumes, and production potential. Additionally, they provide the foundation for simulating fluid flow behavior, thus supporting efficient reservoir management **(Murtazin et al., 2022)**. Formation evaluation integrates electrical, radioactive, and porosity logs with core data to determine mineral composition, shale content, porosity, saturation, and permeability. These parameters define vertical petrophysical profiles along the reservoir interval in each well. These are later extrapolated geostatistically across the unpenetrated areas between wells to construct 3D models representing both structural geometry and the spatial variation of reservoir properties **(Darling, 2005a; Turner et al., 2021)**. It is worth noting that reservoir heterogeneity refers to the vertical and lateral variability in these properties, especially porosity, permeability, and saturation, which directly control fluid-flow behavior and recovery performance **(Al-Dujaili et al., 2023)**.

Ratawi Oil Field is located in southern Iraq, approximately 70 km west of Basrah city. Geographically, it extends between the easting coordinates 705,400 – 696,360 m and the northing coordinates 3,394,183 – 3,373,800 m, as shown in **Fig. 1**. The field was initially identified through gravity surveys in the early 1940s. Subsequently, seismic exploration was conducted by the National Oil Company between 1947 and 1948, which revealed that the field exhibits a dome-shaped, near-symmetrical anticlinal structure. At the crest of the Yamama Formation, the structure spans an area of approximately 27 × 14 km^2. The Yamama Formation represents one of the most significant carbonate reservoirs in southern Iraq and is considered a promising hydrocarbon-bearing interval in the Ratawi Field. Deposited during the Early Cretaceous period, the Yamama Formation is overlain by the Ratawi Formation and underlain by the Sulaiy Formation **(Jassim and Goff, 2006)**. Based on petrophysical interpretations derived from well log analysis, **(Al-Siddiki, 1978)** Subdivided the Yamama Formation into five distinct stratigraphic units: three reservoir units (A, B, and C), separated by two non-reservoir barrier units (C1 and C2).

The Yamama Formation was first described in the Yamama region of Saudi Arabia by **(Steinke and Bramkamp, 1952)**. Shortly thereafter, **(Rabanit, 1952)** Conducted a lithological description of the Yamama/Sulaiy section in well Rt1. In a comparative regional study, **(Dunnington, 1958)** noted that the Yamama Formation was integrated with the Sulaiy Formation, based on the analysis of two wells: Rt1 in southern Iraq and Burgan113 in Kuwait, dividing the formation into six subdivisions. Later, **(Chatton, 1962)** redefined the Yamama and Ratawi formations in well Rt1, distinguishing them based on lithological criteria.

A more detailed petrophysical evaluation was presented by **(AL-Siddiki, 1977)**, who emphasized that the contact between the Yamama and Ratawi formations is conformable. The following year, **(Al-Siddiki, 1978)** proposed a five-unit subdivision of the Yamama Formation based on well log interpretation, delineating three reservoir units (A, B, and C), separated by two non-reservoir barrier units (C1 and C2). In a regional extension **(Roberson, 1979)** in **(Motlaq, 1999)** applied a similar subdivision into three units in the Managish-8 well in Kuwait. While **(Sadooni, 1993)** focused on depositional systems of the formation, dividing it into two main units in wells Rt3, West Qurna, and Kuwait. Later, **(Rozarian, 1995)** proposed a threefold division for the Yamama in Iraq, two reservoir units separated by a sealing unit. In a source rock context, **(Al-Shahwan, 2002)** reaffirmed the formation's potential as a major hydrocarbon source in southern Iraq.

In terms of reservoir characterization**, (Murtadha, 2012)** conducted a formation evaluation in the Ratawi Field based on well log interpretation, confirming a lithology dominated by limestone with minor dolomite and shale components. She estimated the original oil in place (OOIP) to be approximately 2,566 million barrels. Followed by, **(Al-Shahwan and Al-Iessa, 2015)** assessed the petrophysical properties of the Yamama Formation in the Ratawi Field using well log data, concluding that the lower part of unit YB exhibited the most favorable reservoir characteristics. A broader 3D geological modeling study was undertaken by **(ALhakeem et al., 2019)** across three oil fields, where comparative analysis showed that unit YB consistently possessed superior petrophysical attributes in the Ratawi Field. Most recently, **(Al-Iessa and Zhang, 2023)** conducted a multi-faceted investigation to delineate the internal boundaries of Yamama reservoir units in the Ratawi Field. This included qualitative interpretation of log data to identify lithological transitions, quantitative calculation of petrophysical parameters to refine unit boundaries, and detailed microfacies analysis of core samples to validate facies transitions at the subunit level.

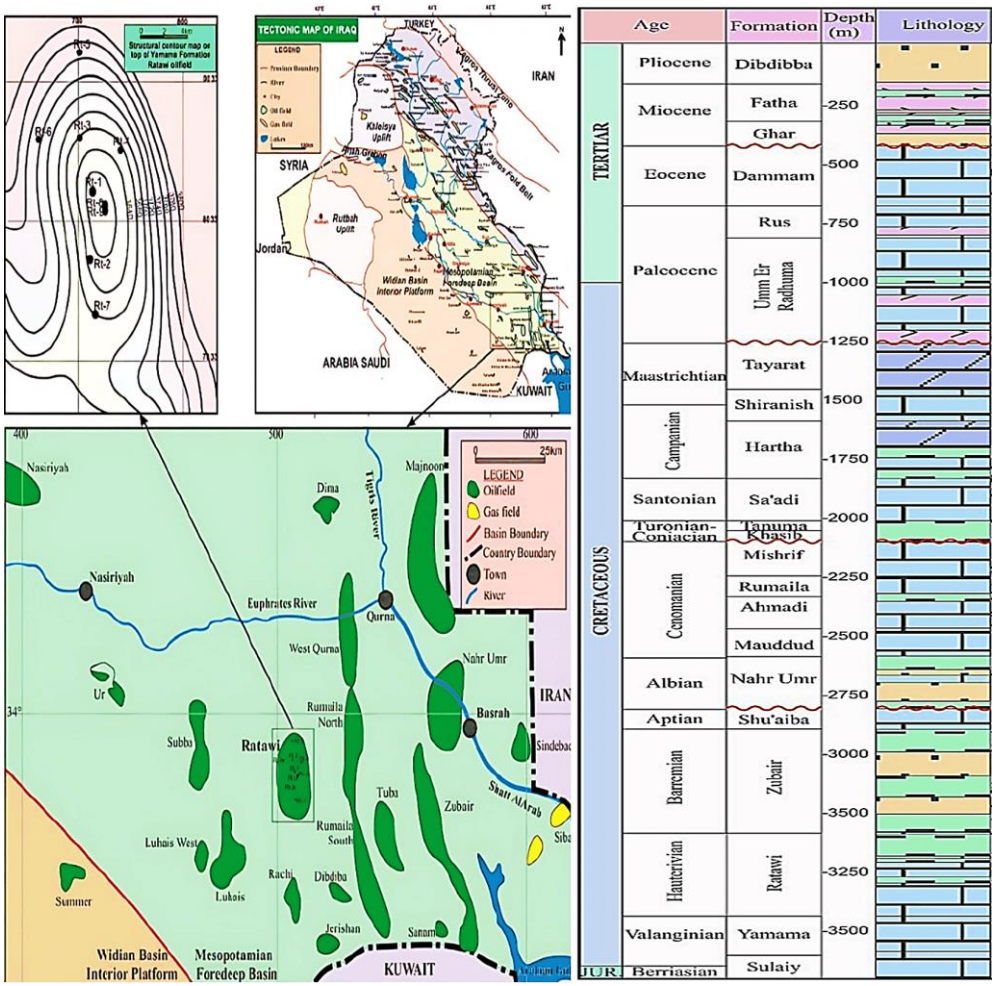

Figure 1. Location map of the Ratawi oil field and stratigraphic section **(Al-Ameri et al., 2015)**.

Reservoir characterization relies on interpreting data acquired at various scales. At the field scale, seismic data are commonly used to define stratigraphic and structural boundaries. At the well scale, logging data represent the primary source for reservoir evaluation, while the core scale provides direct measurements of porosity, permeability, and lithology, thus

serving as a calibration reference for other datasets **(Darling, 2005a)**. Integrating multi-scale datasets facilitates a comprehensive assessment of reservoir formations through the estimation of key concepts, such as Rock Typing and petrophysical properties.

Rock typing is central to grouping formations with similar properties, whether sedimentary (SRT), petrophysical (PRT), or linked to reservoir performance (RRT). Facies correspond to SRT, while flow units reflect PRT **(Kurniawan et al., 2021)**. Facies describe depositional features (e.g., channels, splays, overbank) and provide a broader classification than lithology, which specifies rock composition. Although lithology is more detailed, 3D lithology modeling is rarely practical, whereas facies models can be constructed from core, logs, or seismic data. Core-derived facies are termed lithofacies, integrating composition and depositional environment, while log-derived facies are known as petrofacies or electrofacies and usually require calibration to lithofacies **(Ma, 2019a)**. Facies are inferred from logs through cutoff methods, discriminant analysis, or advanced tools such as Artificial Neural Networks (ANN) trained on log-core data and cluster analysis, which can be enhanced using Principal Component Analysis (PCA) **(Ma, 2019a)**. Complex reservoirs often require multilevel classification **(Ma, 2019a)**. Cluster analysis partitions data into electrofacies using unsupervised algorithms **(Alameedy et al., 2023)**. K-means is widely applied due to simplicity and efficiency with low-complexity data, but requires defining cluster numbers and is sensitive to initial centroids. The workflow involves centroid initialization, data assignment based on minimal distance, recalculating means, and iteration until convergence. Tools such as the Elbow Method, Silhouette Score, and Gap Statistic guide the optimal cluster number **(Akinbode and Samuel, 2025)**. Identifying lithology for primary reservoir units remains crucial to deriving petrophysical properties from logs. This can be achieved directly through core analysis or indirectly via log cross-plots such as Density–Neutron and Neutron–Sonic **(Darling, 2005b)**.

Shale in reservoirs is generally unfavorable as it reduces effective porosity and permeability and lowers resistivity, causing overestimated water saturation (Sw). Correcting water saturation to effective water saturation (Swe) thus requires shale volume (Vsh) estimation. Shale distribution could be as laminated, dispersed, or structural; the latter may not significantly affect porosity but alters log responses. Shale volume is commonly derived from Gamma Ray logs, while resistivity, SP, and porosity logs provide alternatives, though less reliable due to complex shale effects **(Bateman, 2012)**.

Effective porosity is obtained by correcting total porosity from neutron, density, and sonic logs for shale. In clean formations, water saturation is estimated with Archie's model using water resistivity (Rw), true resistivity (Rt), and Archie parameters; in shaly rocks, corrections are required **(Bateman, 2012)**. Correction model selection depends on shale type and distribution: the Indonesian model is used for uncertain shale geometry; Simandoux and variants for complex or moderately shaly carbonates; Waxman-Smits for dispersed shaly sands; and the Dual Water model for laminated/dispersed shale **(Waxman and Smits, 1968; Clavier et al., 1984; Kumar, 2010)**. Key parameters in these models include formation water resistivity (Rw), cementation exponent (m), saturation exponent (n), and tortuosity factor (a). Rw indicates formation water salinity and can be measured in the lab or estimated from logs **(Bateman, 2012)**. Cementation Exponent reflects pore geometry, typically ~2 in sandstones/carbonates, <1 in fractured rocks, and >3 in compacted sandstones **(Salem and Chilingarian, 1999)**. Saturation exponent, linked to wettability and microporosity, is often close to the cementation exponent or derived from

Pickett plots **(Han et al., 2021)**. Tortuosity factor a, describing flow path length, is usually ~1 for carbonates and ~0.62 for sandstones **(Pickett, 1966; Bateman, 2012)**.

Net-to-Gross (NTG), the ratio of reservoir to total rock volume, indicates storage and productivity. It is estimated indirectly by excluding non-reservoir facies or directly through petrophysical cutoffs (e.g., porosity, permeability, Sw). NTG equals effective points meeting cutoffs divided by total points, guiding volumetrics and flow models, though results depend on statistical representativeness **(Ma, 2019d)**. Cutoffs may be tailored to lithofacies to reflect pore-throat variability, improving accuracy **(Egbele et al., 2005)**. In simulations, cells failing cutoffs are excluded, though water saturation cutoffs are avoided as capillary pressure redistributes water saturation **(Ma, 2019d)**.

A geological model is a 3D framework that defines reservoir geometry and distributes key petrophysical properties such as facies, porosity, water saturation, and permeability. It enables evaluation of reservoir heterogeneity, estimation of in-place volumes, and simulation of fluid flow by dividing the reservoir into grid blocks used in dynamic modeling **(Ma, 2019e)**. Common modeling strategies include pixel-based methods, efficient with well data but geologically limited; object-based methods, which capture depositional features but are harder to constrain; and Multiple Point Statistics (MPS), which employs training images to reproduce complex patterns **(Phan, 2002)**. Model construction typically involves structural, stratigraphic, facies, and petrophysical modeling, supported by scale-up of well data into grid cell averages. Property distribution may follow deterministic (single realization), stochastic (multiple realizations), or hybrid approaches **(Cosentino, 2001)**. Geostatistics provides a framework to predict reservoir properties at unsampled points, assuming spatial correlation for known points **(Wang et al., 2025)**. It begins with semi-variogram/Covariance analysis to quantify property similarity with distance (variogram models), followed by kriging interpolation, which uses these variograms to assign weights to known data for optimal prediction **(Zhang, 2009)**. The variogram describes correlation through nugget, sill, and range parameters, with exponential, Gaussian, and spherical models used to fit observed data **(Ma, 2019c)**. Interpolation methods include kriging, which yields deterministic but smoothed results, suppressing natural extremes **(Ma, 2019b)**. Alternatively, sequential Gaussian simulation (SGS) applies kriging mean and variance in a random iterative process, generating multiple realizations that preserve local heterogeneity and spatial uncertainty **(Ma, 2019g)**.

Upscaling is the process of converting a fine-grid geological model into a coarser one suitable for reservoir simulation, while retaining essential geological and hydrodynamic features. This step is necessary because fine models, with their millions of cells, are computationally demanding in long-term simulations. The aim is to reduce grid blocks with minimal loss of accuracy. Studies commonly favor building a detailed model first, followed by upscaling, rather than starting with a coarse model, which often omits critical geological details **(Ma, 2019f)**. Structural upscaling involves merging thin layers and enlarging cells laterally while preserving barriers, faults, and channels. Grid refinement may be retained near wells or complex zones. Petrophysical upscaling transfers porosity, permeability, saturation, facies, and net-to-gross using averaging methods, often sequentially, for instance, scaling porosity on net-to-gross and saturation on both **(Santos et al., 2022)**. Validation compares coarse- and fine-scale volumes (e.g., Pore volume, OOIP) and flow properties to ensure geological and dynamic consistency. Unlike the earlier scale-up of log data to model cells, this upscaling addresses model-wide grid reduction but applies similar averaging principles **(Ma, 2019f)**.

Following a review of the literature, this study aims to evaluate the Yamama Formation in the Ratawi Field, utilizing comprehensive well data to classify facies, assess petrophysical characteristics, and construct a 3D geological model. The model supports estimation of hydrocarbon volumes and identification of zones with variable reservoir quality. The primary objective is to develop an integrated geological model that forms the basis for reservoir simulation. It is evident from the reviewed literature that most prior studies on the Yamama Formation emphasized its geological framework; few have addressed reservoir characterization, and none incorporated data from recently drilled wells (Rt13, Rt14, Rt15). Therefore, this study distinguishes itself by integrating these updated datasets, thereby reducing uncertainty towards improving evaluation accuracy. Moreover, it adopts advanced methodologies that prioritize petrophysical interpretation, offering a more robust and reliable characterization of the reservoir.

2. METHODS AND MODELING

The adopted workflow for evaluating petrophysical properties of the Yamama reservoir in the Ratawi field involved data collection, quality control, and integration into commercial formation evaluation and geological modeling software. Key parameters, shale volume, porosity, water saturation, and permeability, were calculated, while facies were classified through cluster analysis on a programming platform. It should be noted that the permeability estimation method was presented in a separate academic paper, while its distribution within the Yamama reservoir model is incorporated here to deliver a fully integrated, simulation-ready geological model. Results were imported for structural modeling, variogram construction, and geostatistical interpolation to spatially distribute properties. Cells were categorized by net-to-gross cutoffs to support volumetric assessments, followed by OOIP estimation and geological model upscaling to ensure readiness for simulation with acceptable accuracy. The dataset comprised all wells penetrating the Yamama Formation, namely Rt3, Rt4, Rt5, Rt6, Rt7, Rt13, Rt14, and Rt15, excluding the abandoned Rt1 due to incomplete data as shown in **Fig. 2**.

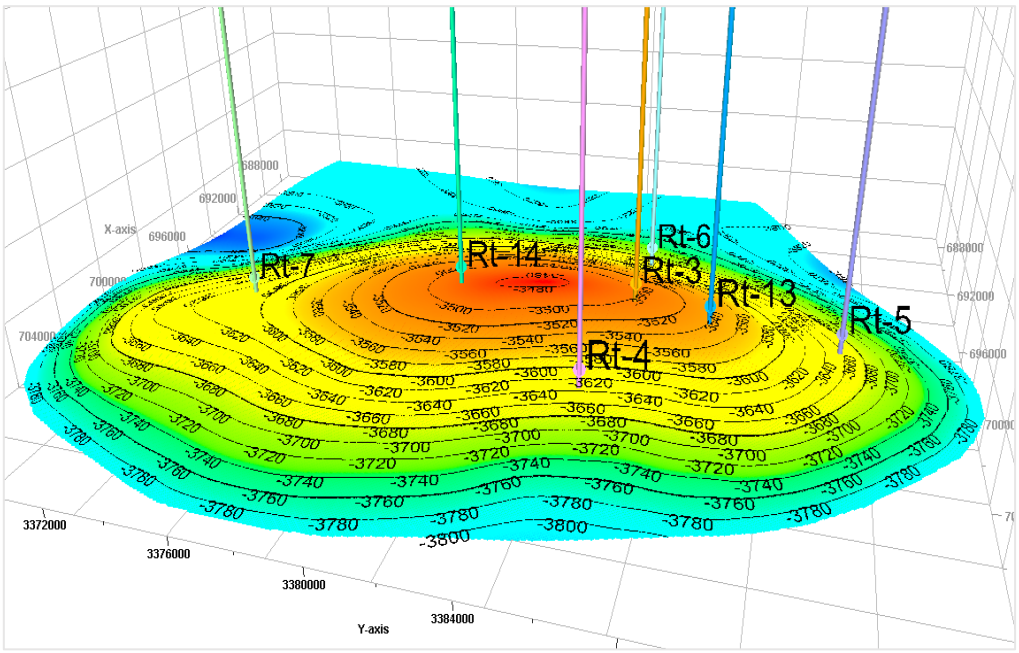

Figure 2. The studied wells that penetrated the Yamama Formation.

Available data included wireline logs, PLT records, slickline measurements, routine and special core analyses, Final Geological Reports (FGRs), Final Drilling Reports (FDRs), completion and perforation reports, DST and production tests, PVT analysis reports, structural maps, and prior studies by the National Oil Company, South/Basra Oil Company, and service companies. Core samples were retrieved from four intervals in Rt3, two in Rt4 (usable data for one), and ten in both Rt5 and Rt6. Although cores existed for Rt7 and Rt14, analysis was unavailable, while no cores were taken from Rt13 and Rt15 as in **Table 1**.
All data underwent rigorous quality control. Wireline logs were merged from multiple runs, poor-quality passes removed, and off-depth errors corrected using the Gamma Ray log as a reference. Environmental corrections addressed borehole conditions (casing, geometry, mud density) via built-in software tools, though their impact was minor due to wellbore stability. Core depths were aligned with log depths, improving porosity consistency, with no further adjustments needed, as core recovery was nearly 100%, typical of carbonates.

Table 1. Core samples provide details of the studied wells.

Well	Cored Intervals (m)	Recovery (%)	Well	Cored Intervals (m)	Recovery (%)	Well	Cored Intervals (m)	Recovery (%)
Rt3	3690 – 3707.5	100	**Rt5**	3788 – 3805.5	100	**Rt6**	3689 – 3706.5	95.7
	3707.5 – 3723.5	100		3805.5 – 3823	100		3780.5 – 3798	83.7
	3724.25 – 3742	97		3823 – 3840.5	100		3798 – 3813	96.7
	3742 – 3760	97.2		3840.5 – 3858.8	100		3813 – 3830.5	99.4
Rt4	3796.5 -3813.5	95.6		3858.5 – 3875.5	100		3830.5 – 3848	96.3
				3875.5 – 3893	100		3848 – 3865.5	98.9
				3893 – 3901.5	100		3865.5 – 3883	100
	3813.5 - 3830.5	100		3901.5 – 3919	100		3883 – 3900.5	100
				3919 – 3936.5	100		3900.5 – 3918	100
	(Not Available)			3936.5 – 3954	97		3918 – 3935.5	99.8

2.1 Petrophysical Properties Determination

Gamma Ray logs records were used in the study wells to estimate shale volume, a key parameter in determining effective petrophysical properties. The Gamma Ray index (IGR) was calculated using Eq. (1), followed by shale volume estimation using the Larionov Older rocks equation Eq. (2), suitable for solidified rocks of the Lower Cretaceous age **(Bassiouni, 1994)**.

$$\text{IGR} = \frac{GR_{log} - GR_{min}}{GR_{max} - GR_{min}} \quad (1)$$

$$V_{sh} = 0.33\left[2^{(2xIGR)} - 1\right] \quad (2)$$

where:
IGR: gamma ray index.
GRlog: gamma ray reading of formation.
GRmin: minimum gamma ray (clean sand or carbonate).
GRmax: maximum gamma ray (shale).
V_{sh}: Shale Volume.

As shown in **Figs. 3 and 4**, shale volumes generally exceed 10% across most intervals, with higher values concentrated at barrier zones separating reservoir units. This distribution is crucial for identifying stratigraphic boundaries within the Yamama Formation and selecting suitable methods for calculating effective porosity in clean and shale-rich intervals. Effective porosity was computed using Neutron and Density logs Eq. (3), with shale volume correction applied using Eqs. (4) and (5), only where shale volume exceeded 10%, as recommended by **(Bassiouni, 1994; Hilchie, 1982)**. This selective correction significantly improved agreement with core-derived porosity, as shown in **Fig. 5** for Cored wells. Since Caliper logs indicated a stable diameter, borehole correction was unnecessary.

$$\emptyset_{ND} = \sqrt{\frac{\emptyset_N{}^2 + \emptyset_D{}^2}{2}} \quad (3)$$

$$\emptyset_{Ncorrected} = \emptyset_N - [V_{sh}\, x\, \emptyset_{Nsh}] \quad (4)$$

$$\emptyset_{DCorrected} = \frac{\rho_{ma}-\rho_b}{\rho_{ma}-\rho_f} - V_{sh}\left[\frac{\rho_{ma}-\rho_{sh}}{\rho_{ma}-\rho_f}\right] \quad (5)$$

where:
$\emptyset_N$: neutron-derived porosity.
$\emptyset_{Ncorrected}$: porosity of neutron log is corrected by the shale effect.
$\emptyset_{Nsh}$: neutron porosity of nearby shale.
Φ_D: density-derived porosity.
$\Phi_{Dcorrected}$: porosity calculated from density log and corrected by shale effect.
ρ_{ma}: matrix density (2.71 g / cm^3 for the studied case, i.e., limestone).
ρ_b: the total formation density (the log reading).
ρ_f: fluid density (1 g / cm^3, fresh fluid, and 1.1 g / cm^3, salty fluid).
ρ_{sh}: the total density of nearby shale.

Secondary porosity index (SPI) was calculated using Schlumberger's 1997 model Eq. (6), based on the Sonic log, which reflects only primary porosity. Shale volume correction was again limited to intervals with shale volume greater than 10% Eq. (7). SPI values ranged from low to negligible due to the contrasting effects of diagenesis, as confirmed in a previous study **(Al-Iessa, 2012)**. Effective porosity averaged between 6% and 13%, consistent with owner reports, as seen in **Figs. 3 and 4**.

$$SPI = \emptyset_{ND} - \emptyset_S \quad (6)$$

$$\emptyset_{SCorrected} = \frac{\Delta_{tlog}-\Delta_{tma}}{\Delta_{tf}-\Delta_{tma}} - V_{sh}\left[\frac{\Delta_{tsh}-\Delta_{tma}}{\Delta_{tf}-\Delta_{tma}}\right] \quad (7)$$

where:
SPI: secondary porosity index.
$\emptyset_s$: sonic-derived porosity.
$\emptyset_{sCorrected}$: porosity calculated from acoustic log is corrected by the shale effect.
Δ_{tlog}: interval transit time in the formation measured by the log (μsec/ft).
Δtma: interval transit time in the rock matrix (47.6 μsec/ft for the studied case, i.e., limestone).
Δ_{tf}: interval transit time through the fluid (189 μsec/ft, fresh fluids, and 185μsec/ft, salty).
Δ_{tsh}: interval transit time in nearby shale.

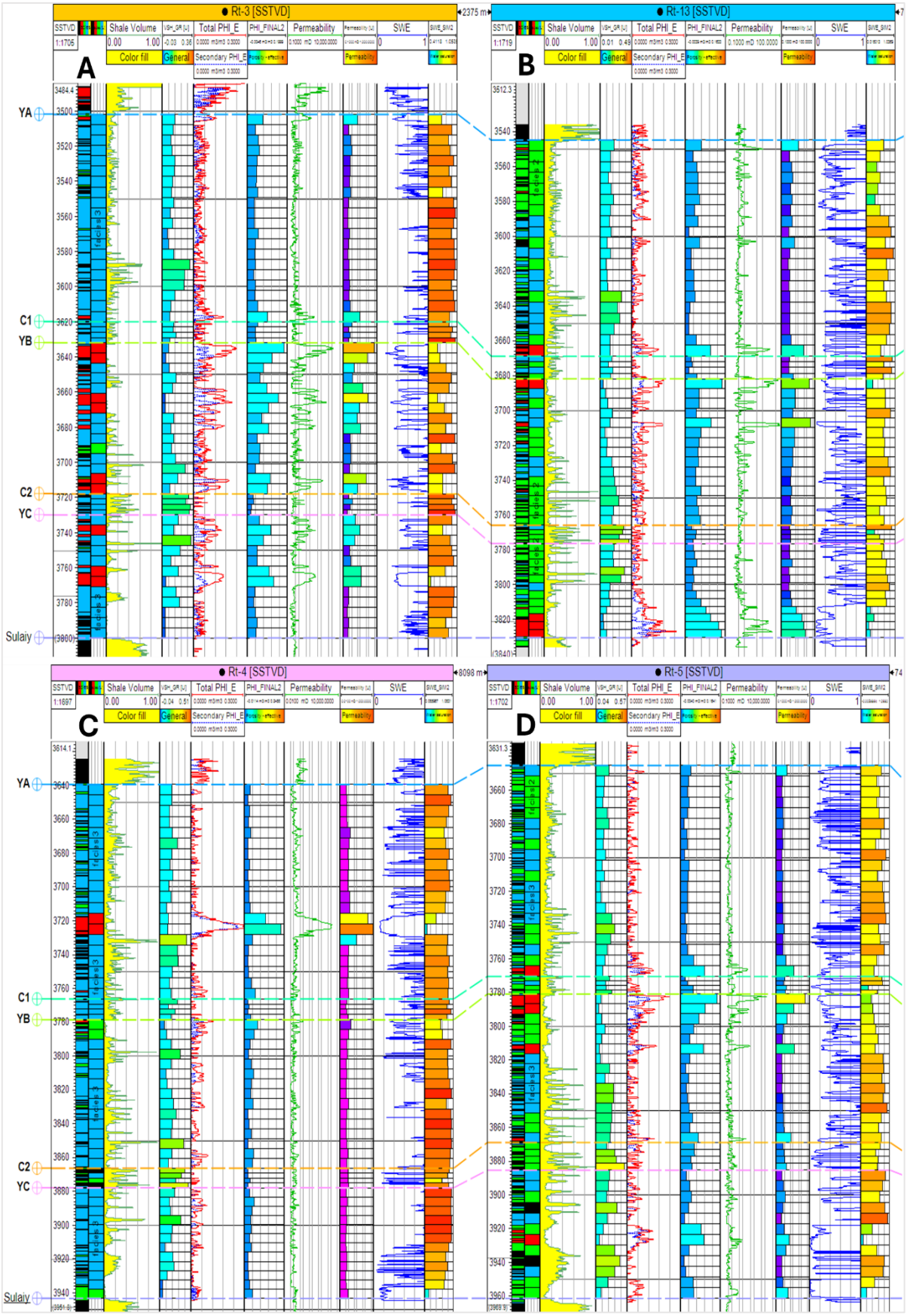

Figure 3. Petrophysical properties and its scale up for; (A) Rt3, (B) Rt13, (C) Rt4, (D) Rt5.

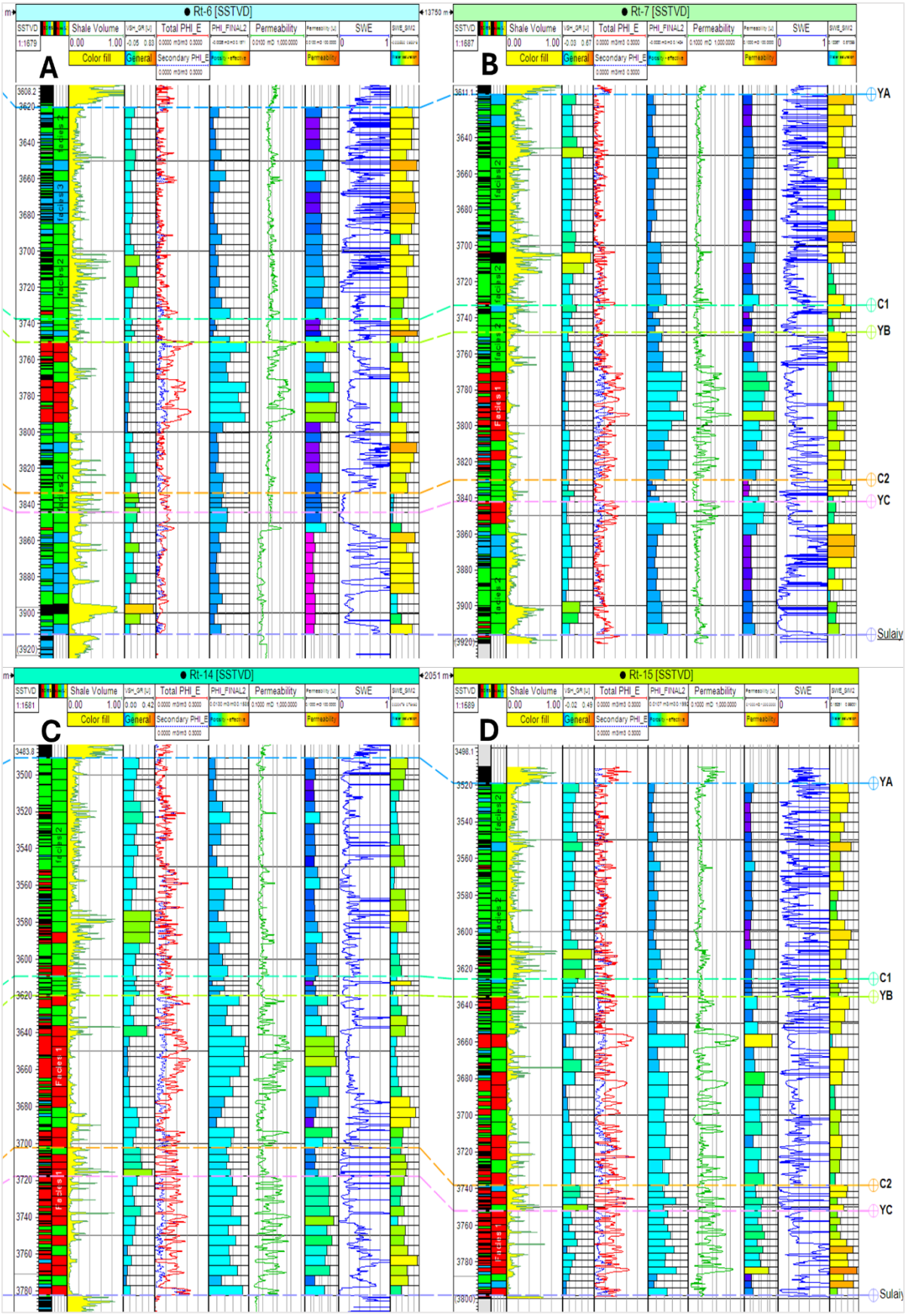

Figure 4. Petrophysical properties and its scale up for; (A) Rt6, (B) Rt7, (C) Rt14, (D) Rt15.

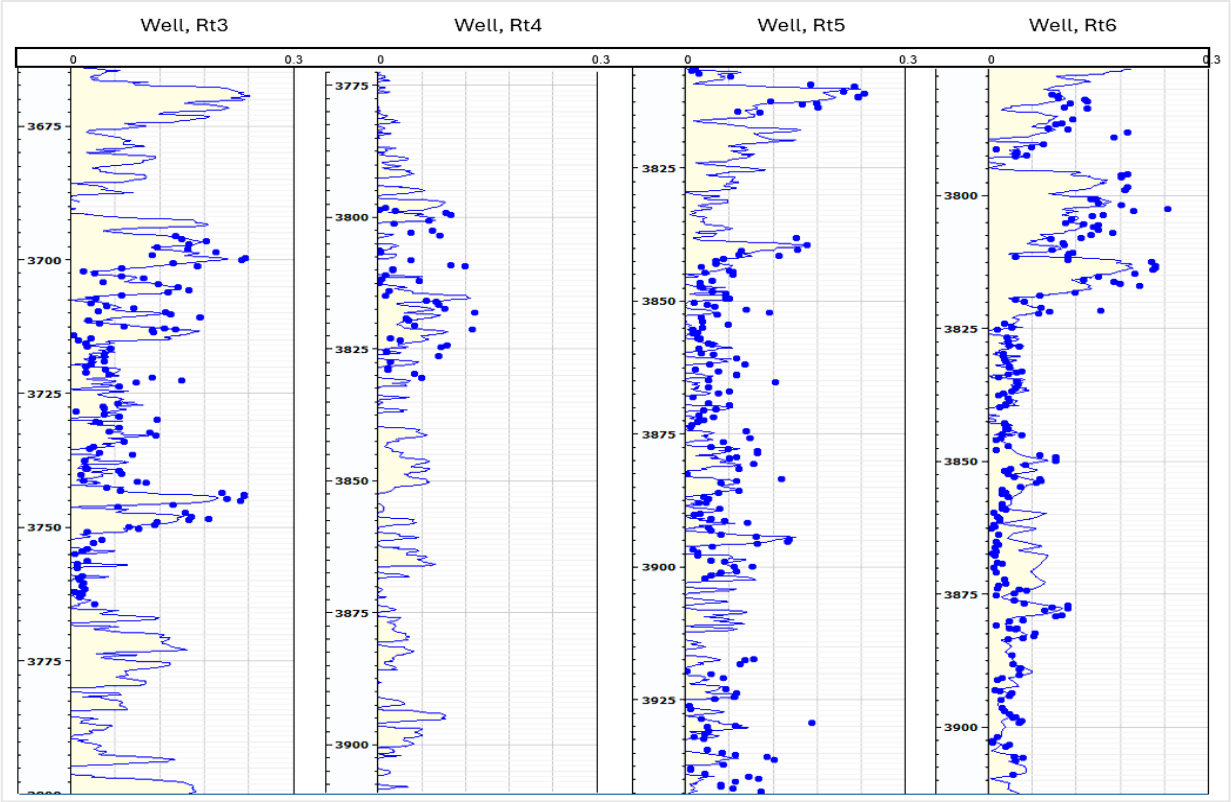

Figure 5. Calculated effective porosity with core-derived porosity of the studied wells.

Subsequently, the Simandoux model Eq. (8) was used to compute water saturation across both clean and shaly zones. In clean intervals, it reduces to the Archie equation **(Kumar, 2010)**. The model yielded consistent results **Figs. 3 and 4**, supporting its applicability in moderately shaly carbonates.

$$S_w = \frac{a\,R_w}{2\,\emptyset^m}\left(\sqrt{\left(\frac{V_{sh}}{R_{sh}}\right)^2 + \frac{4\emptyset^m}{a\,R_w\,R_t}} - \left(\frac{V_{sh}}{R_{sh}}\right)\right) \quad (8)$$

where:

S_w: water saturation of uninvaded zone.

R_w: formation water resistivity (Ω. m).

Ø: porosity (%).

R_{sh}: true or deep resistivity of nearby shale (Ω. m).

R_t: true or deep resistivity of uninvaded zone (Ω. m).

a: tortuosity factor (~1, for studied case i.e. Carbonate).

m: cementation exponent (~2, for studied case i.e. Carbonate).

Key parameters were derived from logs, including true resistivity (Rt), porosity (ϕ), and shale volume (Vsh). Due to high Rmf/Rw ratios (>3) from fresh-water-based mud in most wells, Laterolog tools were unsuitable; thus, Induction Resistivity logs were used **(Bateman, 2012)**. Carbonate rock constants, tortuosity (a = 1) and cementation (m = 2), were adopted from standard values. Shale parameters (ϕNsh, ρsh, Δtsh and Rsh), and Rw were taken from official logging reports. Since these matched values from **(Al-Iessa, 2012; Alhakeem, 2019)**, recalculation was unnecessary.

2.2 Lithology and Facies Determination

Cross-plots of Neutron/Density and Neutron/Sonic logs, combined with lithology charts from service companies, were employed to identify lithology and assign appropriate rock matrix parameters essential for petrophysical calculations, as this widely used method reliably predicts lithology from well logs c. These findings were validated against previous studies, drill cuttings descriptions, and core analyses reports. The Yamama Formation's productive units were predominantly carbonate, specifically limestone, as confirmed by core and geological reports. Data points deviating from the limestone curve, as shown in **Fig. 6** (exemplified by well Rt3). Some points aligned near the dolomite curve, particularly in the lower part of the YB reservoir unit, which also exhibited elevated shale volumes. This aligns with the previous microfacies study **(Al-Iessa, 2012)**, describing YB as dolomitized limestone, peloidal grainstone interbedded with thin shale layers. Similarly, **(Murtadha, 2012)** characterized Yamama lithology as mainly limestone with minor dolomite and shale. While points near the sandstone curve mostly occurred in the unit C2, also **(Al-Iessa, 2012)** identified silica minerals indicative of sandstone lithology.

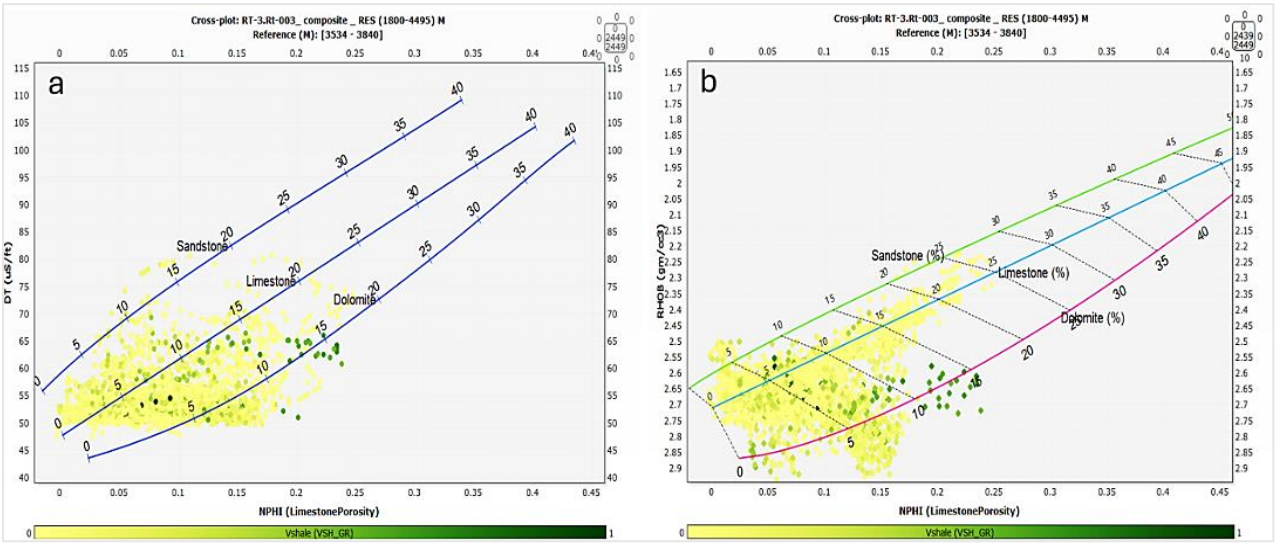

Figure 6. Cross plots of (Rt3); (a) Neutron-Sonic, (b) Neutron-Density of lithology.

Subsequently, K-means clustering classified facies based on calculated petrophysical properties, effective porosity, water saturation, and shale volume from the studied well logs. These facies classifications formed the basis for distributing properties in the geological model. K-means was chosen for its simplicity and effectiveness with low-overlap data **(Akinbode and Samuel, 2025)**. The optimal number of clusters was determined by the Gap Statistic method, which evaluates clustering dispersion against a reference distribution to identify the best cluster count **(Tibshirani et al., 2001)**. As referred to in the introduction, the largest gap occurred at four clusters, which were thus adopted in **Fig. 7**.

Fig. 8, illustrates data distribution and average petrophysical properties per facies. Facies-1 exhibited superior reservoir qualities, whereas Facies-0 had the poorest, typically corresponding to high-shale barrier zones. This is further evident in **Figs. 3 and 4**, where Facies-0 aligns with intervals of the increased shale and impermeable layers, contrasting with the more favorable characteristics of other facies.

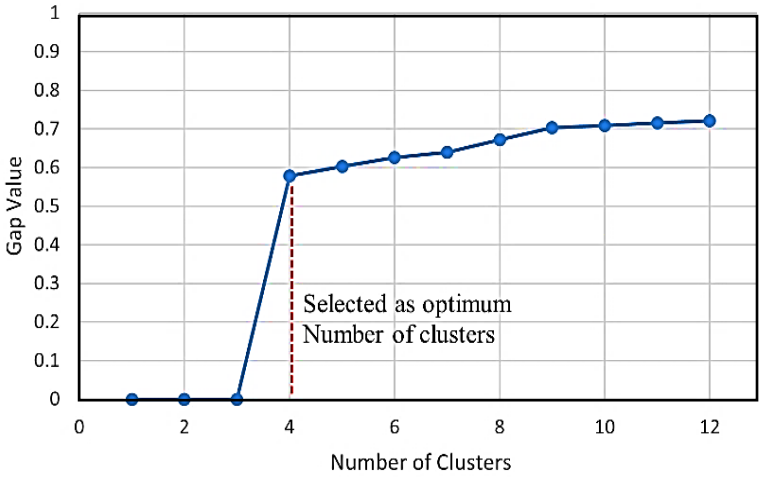

Figure 7. The selection of the Optimum Number of Clusters.

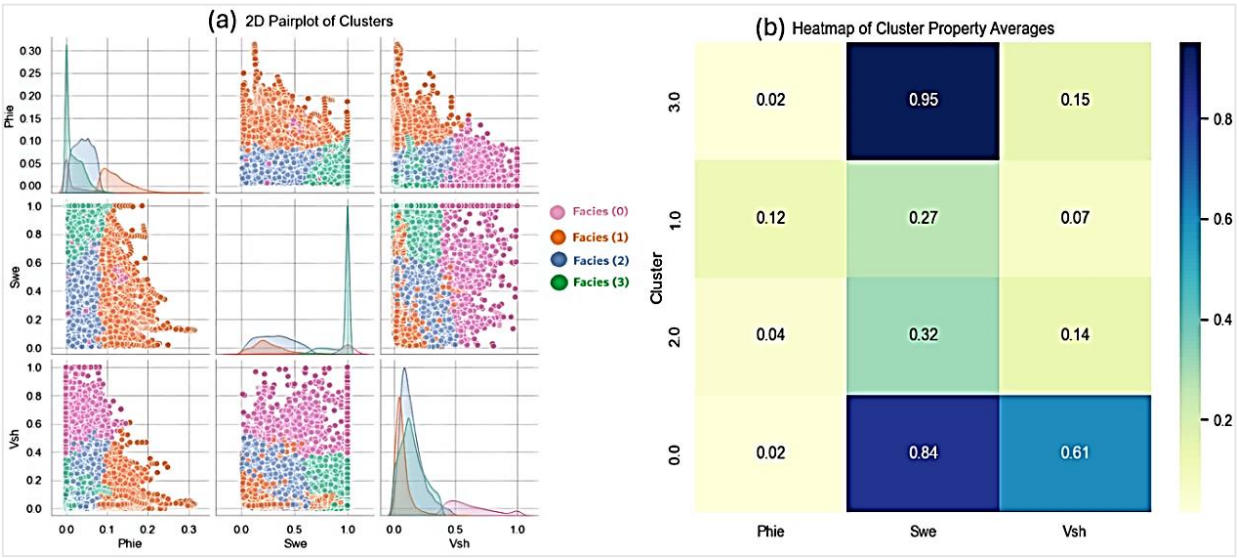

Figure 8. Data distribution and average petrophysical properties per facies; (a) Pair plot of Clusters (Facies), (b) Heatmap of its Property averages.

2.3 Geological Modeling

Geological modeling integrates surface maps and log interpretation results (e.g., facies, porosity, permeability, water saturation) to construct a 3D representation of the reservoir framework. This is achieved using commercial software by importing CPI outputs, structural maps, well locations, tops, and related geological inputs. The well correlation panels (**Figs. 3 and 4**) display the imported log interpretations in 2D to guide property distribution across the 3D model domain. In the structural and stratigraphic modeling stage, the 3D structural model is constructed using the formations of the contour map to delineate horizontal limits via outer-boundary polygons. Vertical boundaries (top depths), were derived from well tops due to limited seismic coverage. Six surfaces were defined: three reservoir units (YA, YB, YC), two intra-formational barriers (C1, C2), and the Sulaiy Formation below.

These surfaces also mark the bounding contacts with the overlying Ratawi and underlying Sulaiy formations (**Fig. 9a**). Well top data were sourced from **(Al-Iessa and Zhang, 2023)**,

which combined log data with core-based microfacies analysis, yielding stratigraphic picks consistent with owner field reports, and supported by log interpretations in this study, as seen in **Figs. 3 and 4**. A 50×50 m^2 horizontal grid was applied, followed by constructing three skeleton surfaces: top, base, and middle (**Fig. 9b**). Vertical gridding (layering) subdivided each zone (reservoir or barrier) into multiple parallel layers to enable accurate property distribution and numerical simulation. This was guided by the scale-up of well data and optimized iteratively. In this model, 55 layers were generated through scale-up procedures intersecting with skeletons to define the final grid structure. Maximum grid dimensions reached 246×472×55, yielding a total of 4,547,840 cells (**Fig. 9c**).

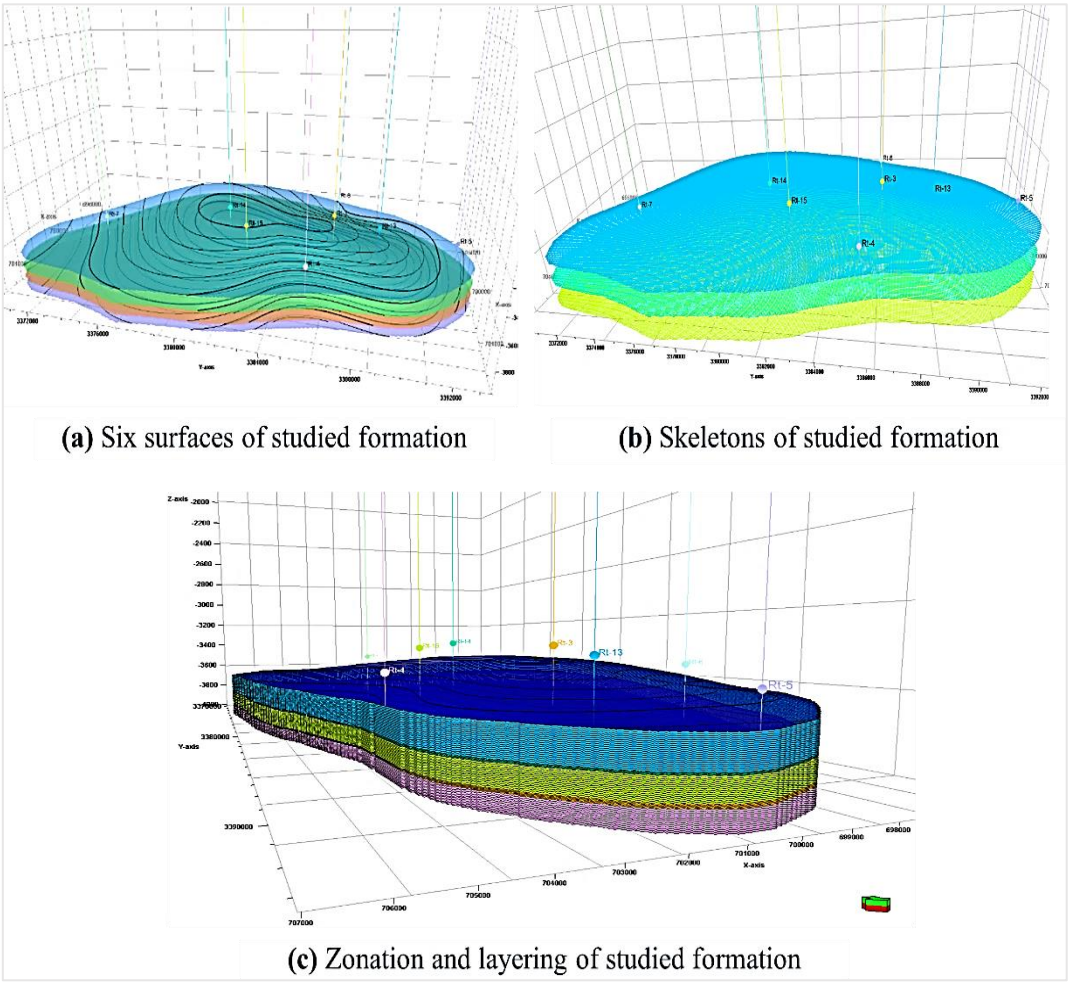

Figure 9. Structural and Stratigraphic Model; (a) Surfaces, (b) Skeletons, (c) Zonation.

Following the construction of the structural framework, petrophysical properties from well logs were scaled up and distributed across the model grid through facies and property modeling. As well, data is sampled more finely than the grid thickness, a scale-up process was applied to convert depth-based point data (facies and petrophysical properties) into single values per grid cell adjacent to each well, facilitating their propagation across the model **(Schlumberger, 2018)**. Facies data were scaled up using the "most of" method, yielding vertical profiles closely aligned with the original facies' distribution. Petrophysical properties (porosity, water saturation, and permeability) were scaled using the root mean square (RMS), offering high consistency with original statistics and trends post-scale-up.

This process also guided the selection of the optimal layer counts within each zone. The accuracy of the scaling-up process is shown in **Figs. 3 and 4**.

Next, variogram modeling and Kriging interpolation were applied for distributing facies and petrophysical properties across all grid cells. Scaled-up data were transformed into a normal distribution using the normal score transformation. These transformed datasets were then analyzed to construct experimental variograms in three directions (vertical, major, and minor), by adjusting the orientation and dimensions of an ellipsoidal search neighborhood, and defining lag intervals. Each facies in every zone had its own variogram model to best reflect spatial continuity, minimizing nugget effects and maximizing range. Petrophysical properties were similarly treated, with models built separately for each facies-zone combination. This approach generated multiple variogram models capturing variability across the field. The outputs included normal-score-transformed data and facies/property-specific variograms for use in the subsequent modeling stage **Fig. 10**. Subsequently, Facies were distributed using Kriging, with each zone handled separately. The Sequential Gaussian Indicator Simulation (SGIS) method was used due to its suitability for categorical data, while Ordinary Kriging was preferred over simple Kriging for its ability to estimate local means more accurately **(Schlumberger, 2018)**. Similarly, porosity, water saturation, and permeability were distributed using Sequential Gaussian Simulation (SGS) based on the corresponding variogram models for each facies in each zone. The previously computed data transformations and variograms were utilized, and Ordinary Kriging was again applied for accurate local estimation, as in the facies case.

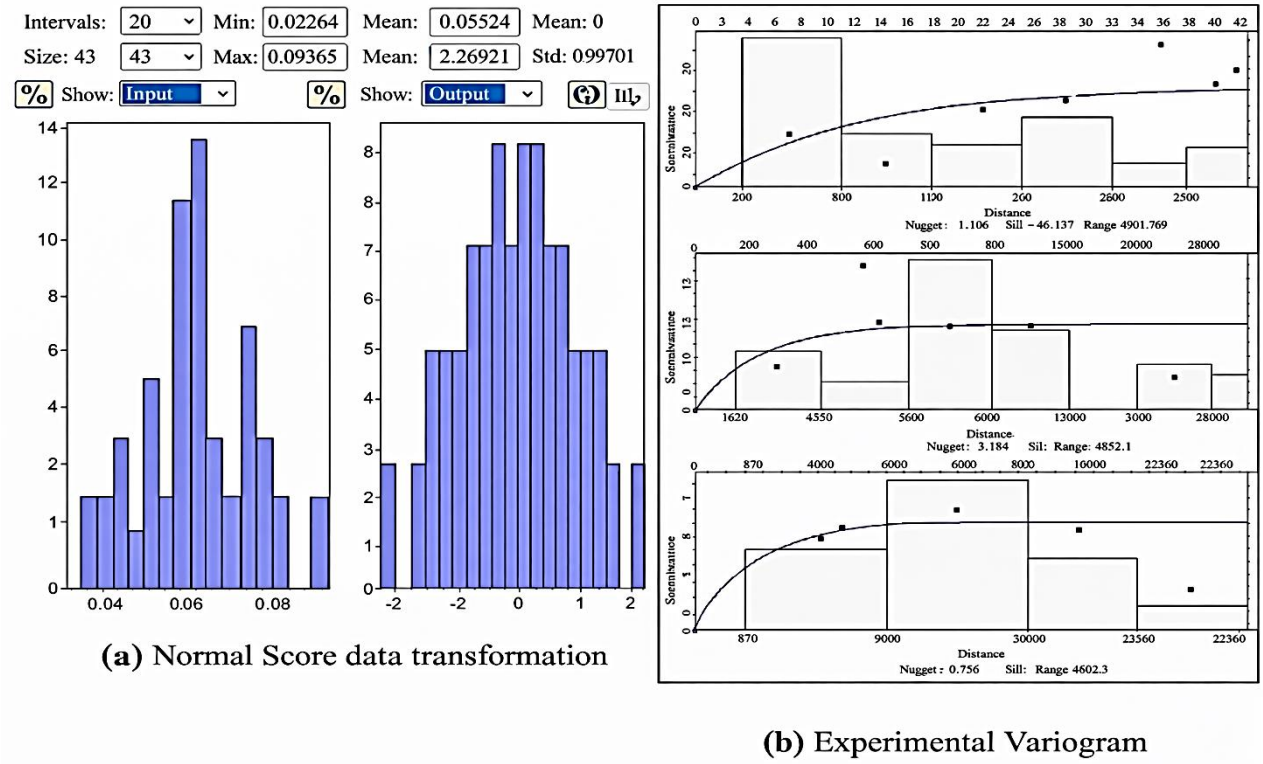

Figure 10. Data transformation and Variogram for porosity (zone YB and Facies 2); (a) Normal score data transformation, (b) Experimental variogram.

2.4 Volumetric Estimation

Following the distribution of petrophysical properties across the geological model grid, porosity and water saturation. Cutoffs were applied to classify cells as reservoir (1) or non-reservoir (0). This classification allows for excluding non-contributing cells from hydrocarbon volume calculations **(Khamees and Abdulrazzaq, 2024)**. For simulation purposes, NTG was alternatively defined by excluding Facies (0) (shale facies) cells, previously classified in this study, by marking them as null cells (inactive). The adopted cutoff values (6% porosity and 45% water saturation) were based on operator field studies by **(TotalEnergies, 2021)** and closely aligned with prior academic findings as **(Alhakeem, 2019; Al-Iessa, 2012)**. In the absence of production or pressure data, volumetric methods offer a reliable initial estimate of Original Oil In Place (OOIP) **(Khamees and Abdulrazzaq, 2024)**. They require only well logs, core analyses, and geological maps. OOIP can be estimated either numerically, by summing individual active cell pore volumes, or analytically using average petrophysical properties and NTG, as in Eq. (9) **(Ma, 2019d)**. This study calculated OOIP for the Yamama reservoir using the derived NTG, petrophysical properties, fluid data, and contact depths from owner reports (OWC; 3820 m). The estimated value, approximately (1800 MMSTB), closely matched the Operator's estimation (1693.4 MMSTB), confirming the validity of the workflow.

$$OOIP = \frac{V_b .\emptyset .NTG .(1-S_{wi})}{B_{oi}} \quad (9)$$

where:
OOIP: original Oil in-Place.
V_b: bulk volume (m^3).
$\emptyset$: porosity (fraction).
NTG: net-to-gross ratio (fraction).
S_{wi}: initial water saturation (fraction).

2.5 Upscaling of Geological Model

The model grid was upscaled horizontally from 50×50 m to 200×200 m, without changing vertical layering to retain heterogeneity accuracy. Petrophysical properties (porosity, permeability, saturation, shale volume, and facies) were transferred using suitable methods: 'Root Mean Square Averaging' for continuous properties, and 'Most of' for facies and NTG. Upscaling accuracy was verified through distribution comparisons (**Figs. 11 and 12**), statistical summaries **Table 2**, and pre-/post-upscaling volumetric estimates of approximately (1,800 MMSTB) and (1,530 MMSTB), respectively, all showing close agreement and validating the coarse model's reliability.

Table 2. Statistics of the Petrophysical properties Upscaling, for all formation units.

	Porosity (%)		Water Saturation (%)		Permeability (mD)	
	Pre-Upscaling	**Post-Upscaling**	**Pre-Upscaling**	**Post-Upscaling**	**Pre-Upscaling**	**Post-Upscaling**
Mean	0.055	0.057	0.61	0.62	7	9
Max	0.24	0.238	1	1	830	795
Min	0.01	0.01	0.001	0.001	0.001	0.016
Var.	0.0013	0.001	0.059	0.043	1782	1758
St.dev.	0.035	0.032	0.24	0.21	42.09	41.93

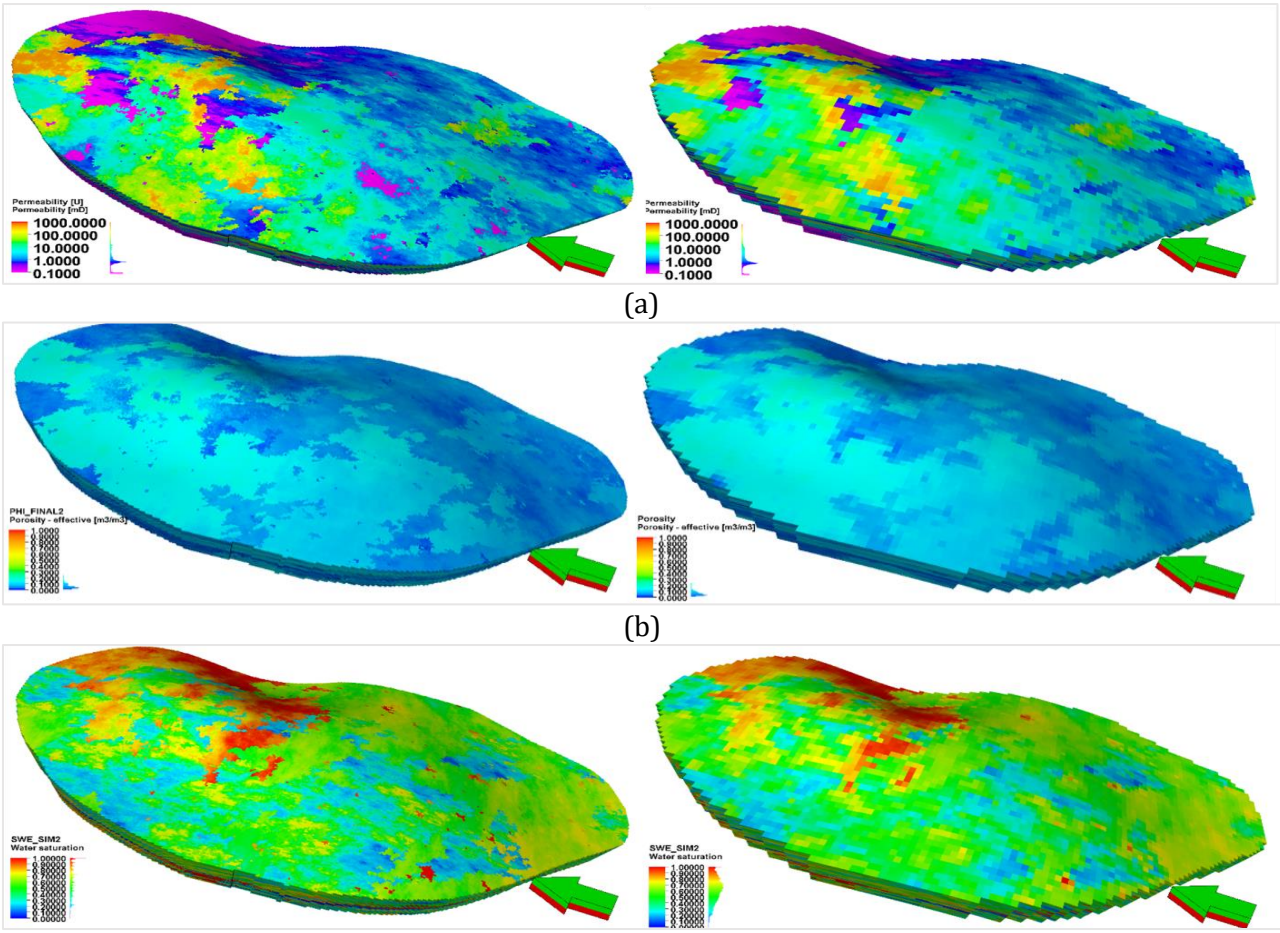

Figure 11. Pre/Post upscaling of petrophysical properties for the top of zone YB; (a) Permeability, (b) Porosity, (c) Water saturation.

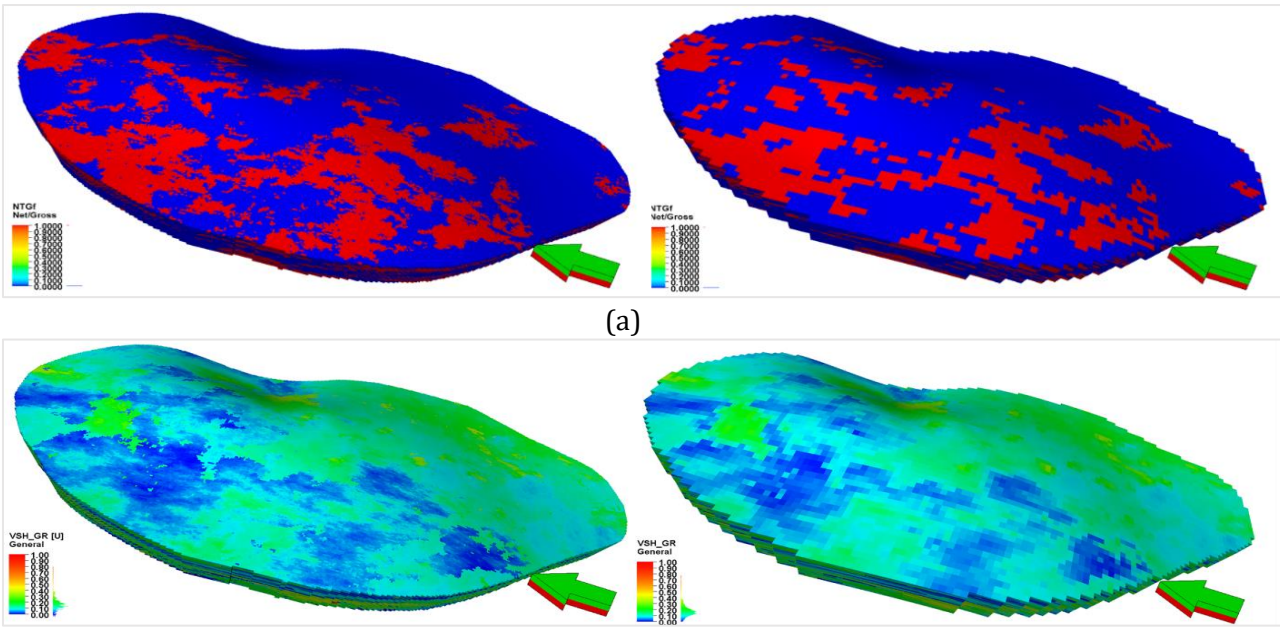

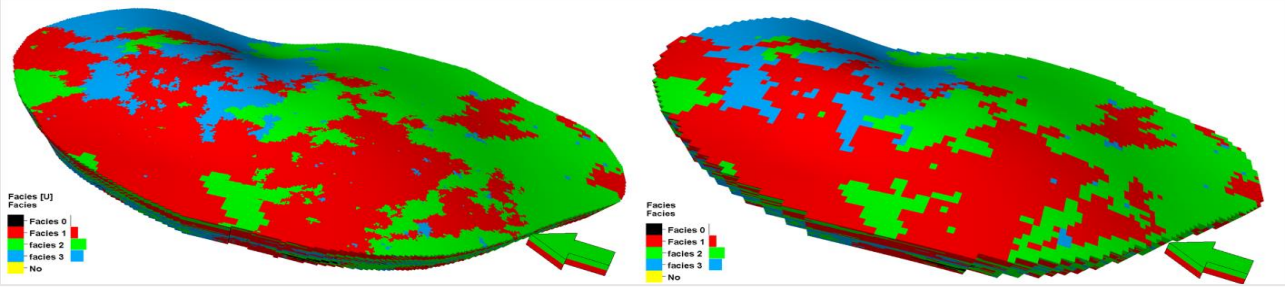

(c)

Figure 12. Pre/Post upscaling of classification properties for the top of the zone YB; (a) Net to Gross Ratio, (b) Shale Volume, (c) Facies distribution.

3. RESULTS AND DISCUSSION

The petrophysical properties of the Yamama Formation in the Ratawi Field, as illustrated in **Figs. 3 and 4** and **Figs. 13 to 16**, reveal distinct vertical and areal heterogeneities that strongly influence reservoir performance. Shale volume increases markedly within the non-reservoir units C1 and C2, at the formation boundaries, and in the lower part of YA, aligning with previous findings. Across most of the formation, shale content exceeds 10%, necessitating log-response corrections. Earlier work, particularly **(Al-Iessa, 2012)**, attributed the classification of C1 and C2 as non-reservoirs to both shale content and compact limestone fabric; however, the present study refines this classification by integrating data from all wells penetrating the formation, providing a more comprehensive spatial validation of these characteristics than was possible in earlier, spatially limited datasets.

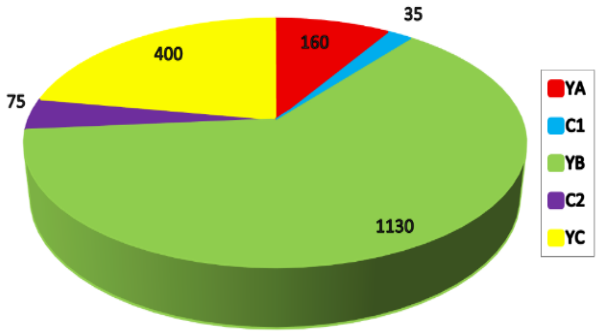

Figure 13. Estimated OOIP for each unit in the Yamama Formation.

Porosity ranges between 6–13%, while permeability spans 0.2–600 md; shale-rich or tight intervals rarely exceed 6% porosity and 0.2 md permeability, confirming limited reservoir contribution. Permeability and effective porosity are moderate at the top of the formation but increase toward the northwestern and northeastern flanks, decreasing eastward and southward. Secondary porosity is generally minor, with its highest development at the top (Rt3) and northeastern flank (Rt4), supporting total porosity; its notable reduction at Rt5 likely reflects post-depositional cementation. **Figs. 14 and 15** reaffirm the superior reservoir quality of YB, exhibiting significantly higher porosity and permeability than YA and YC. Water saturation is elevated in the lower YA, indicating poorer hydrocarbon saturation, whereas YB shows more favorable saturation across central, northwestern, and southern sectors. YC demonstrates moderate water saturation, particularly along the southern flank **Fig. 16**.

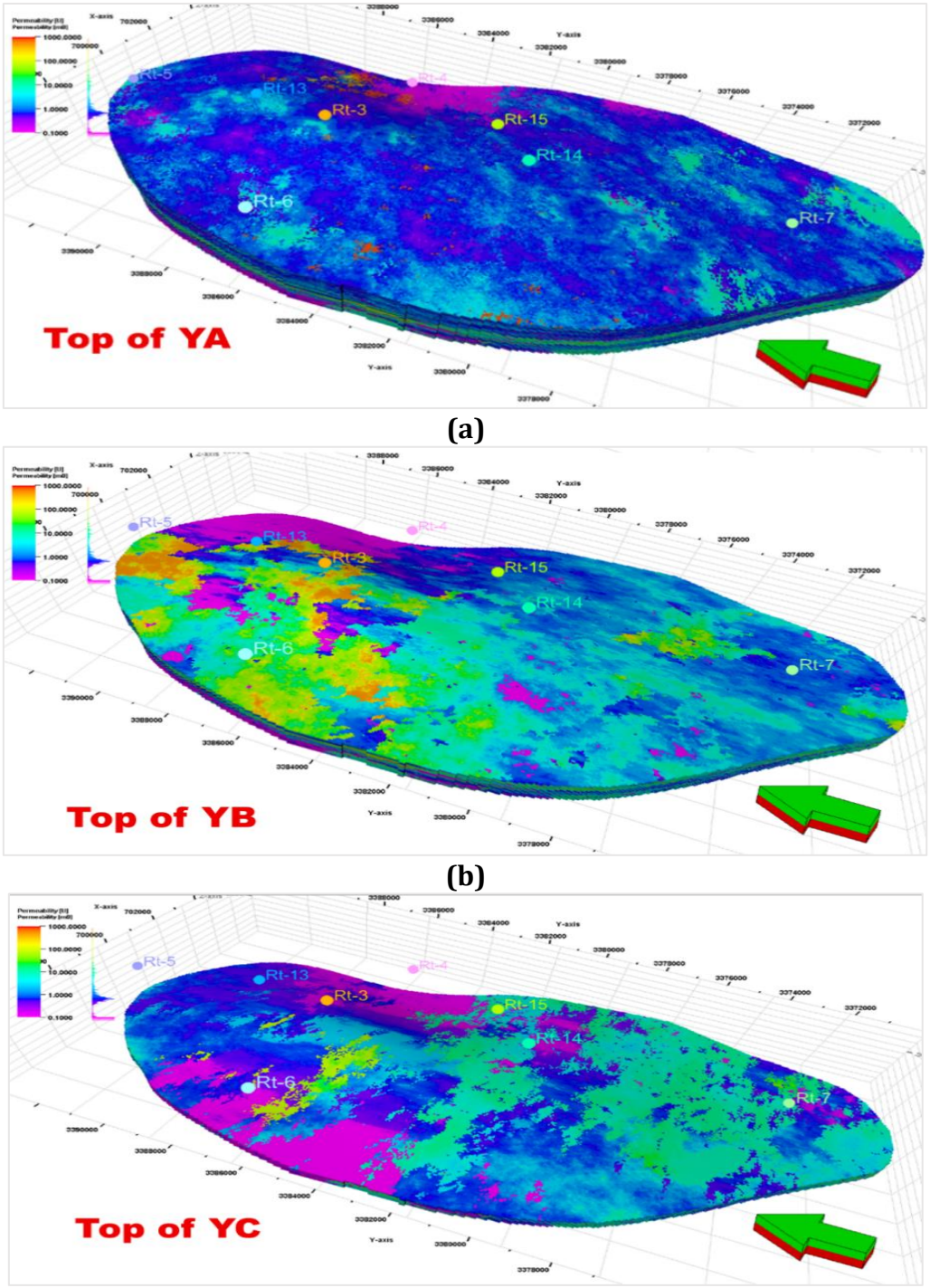

Figure 14. Permeability distribution for the top of Yamama reservoir Units; (a) Top of YA, (b) Top of YB, (c) Top of YC.

OOIP estimates as in **Fig. 13**, identifying YB as the most hydrocarbon-rich unit, followed by YC, while YA contributes minimally. Units C1 and C2 remain economically insignificant due to low permeability and limited thickness. Overall, YB stands out as the most prospective reservoir interval, combining superior porosity, permeability, net-to-gross, and lower water saturation. The poorer quality of the lower YA results from high shale content and suboptimal saturation. Spatially, reservoir quality improves toward the northwest and

declines eastward, highlighting the importance of net-pay distribution for development-well placement.

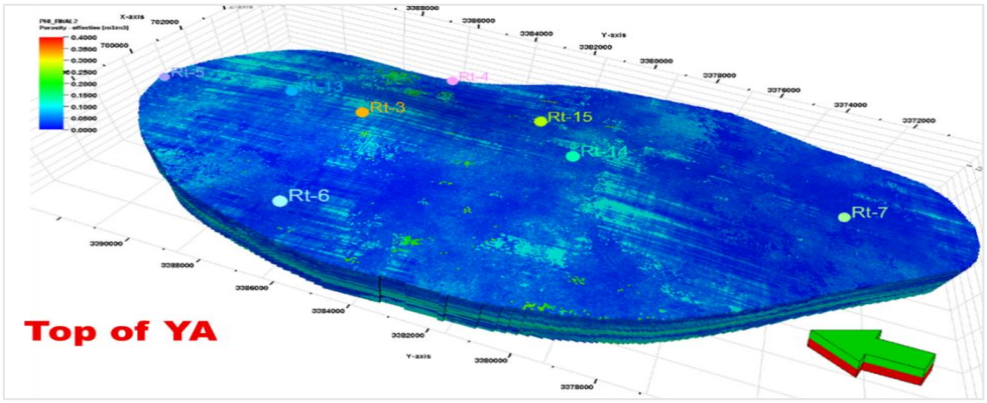

(a)

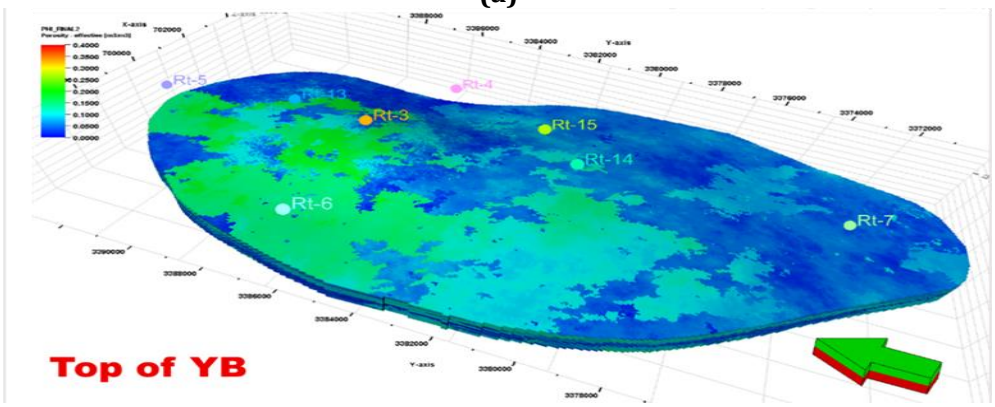

(b)

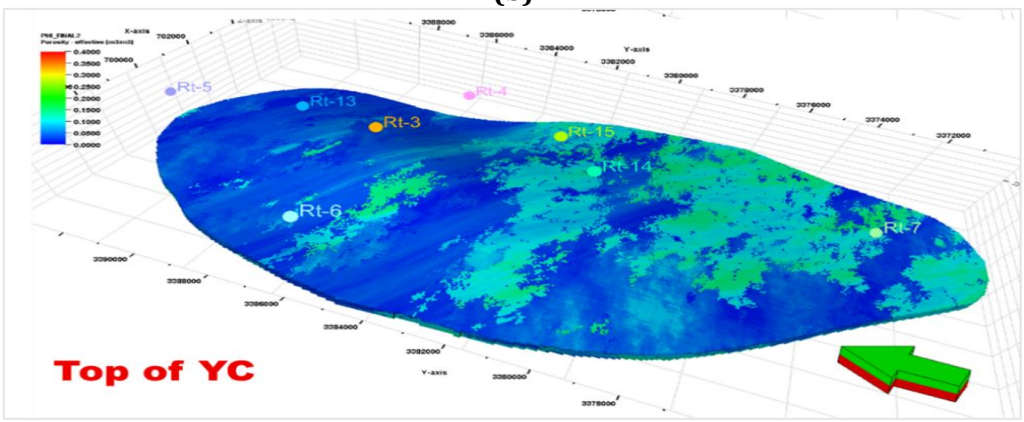

(c)

Figure 15. Porosity distribution for the top of Yamama reservoir Units: (a) Top of YA, (b) Top of YB, (c) Top of YC.

These findings remain consistent with earlier studies **(Murtadha, 2012; Al-Iessa, 2012; Alhakeem, 2019)**; however, the present work provides a more robust spatial interpretation given its geological model constructed from all wells intersecting the formation, enabling full-field distribution of properties rather than relying on narrow well control. Moreover, this study further distinguishes itself by applying facies-based geostatistical property distribution, yielding more realistic reservoir representations and closer alignment with multiple field reports and studies compared with earlier non-facies-constrained evaluations.

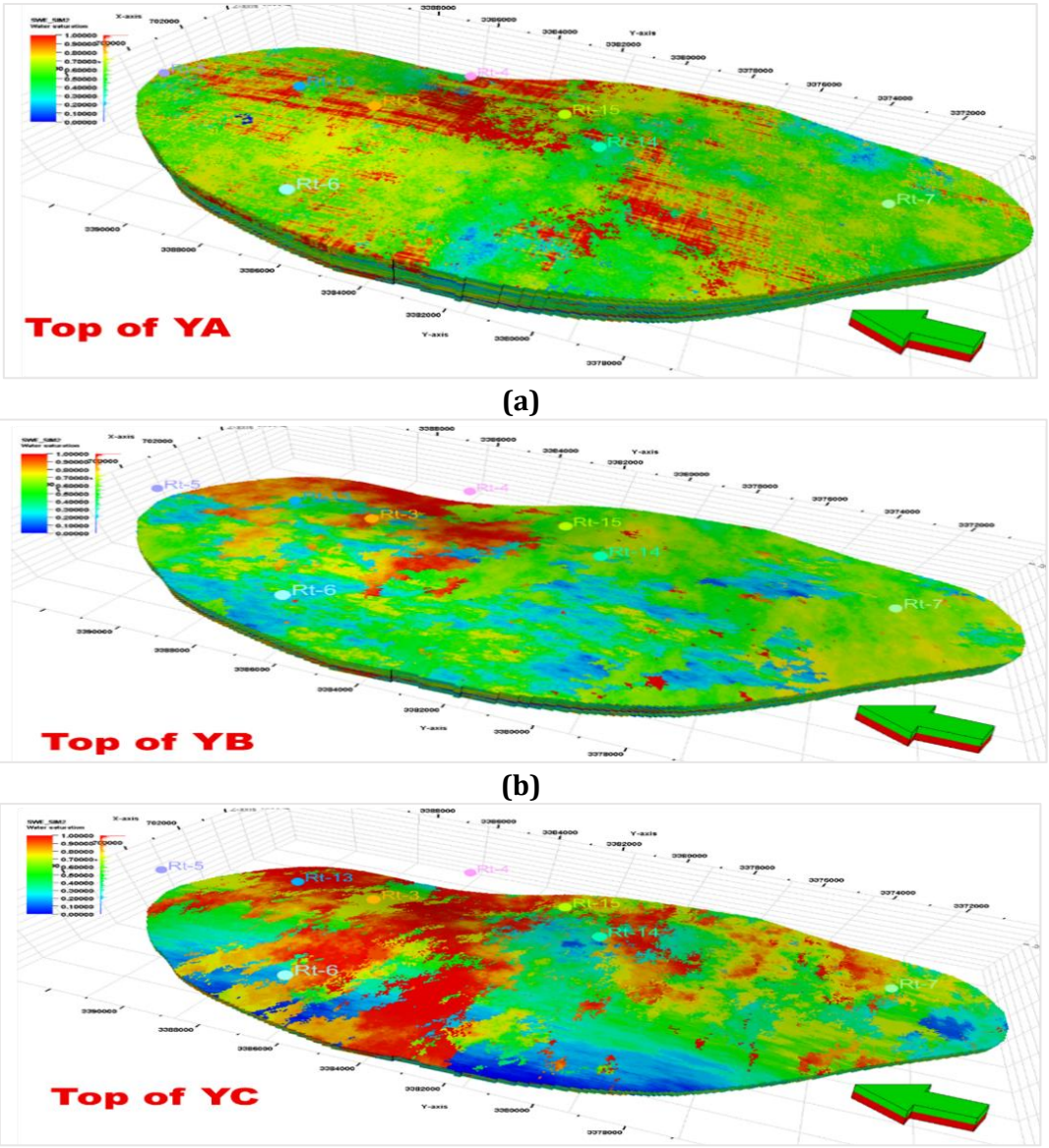

Figure 16. Water saturation distribution for the top of Yamama reservoir Units: (a) Top of YA, (b) Top of YB, (c) Top of YC.

4. CONCLUSIONS

This study provided an integrated characterization of the Yamama Formation in southern Iraq, evaluating shale volume, porosity, water saturation, and permeability while constructing a fully simulation-ready geological model informed by detailed facies interpretation. These efforts delivered a more complete and field-representative understanding than earlier, more limited assessments. The principal conclusions are as follows:

1. The Yamama Reservoir exhibits pronounced vertical and lateral heterogeneity, comprising five units with carbonate-dominated lithology interbedded with shale, particularly in C1, C2, and the lower YA, which diminishes reservoir quality. Petrophysical parameters fall within ranges of 6–13% for porosity and 0.2–600 md for permeability, reinforcing the contrast between reservoir and non-reservoir intervals.

2. Reservoir quality improves toward the top of the formation and along the northwestern and southern flanks, where porosity and permeability increase and water saturation decreases, whereas an evident deterioration occurs eastward. Among the reservoir units, YB exhibits the most favorable properties and highest hydrocarbon content (~63% OOIP), YC shows moderate quality, and the lower YA remains compromised by elevated shale and poor saturation.
3. The total original oil in place (OOIP) is estimated at approximately 1,800 MMSTB, in agreement with operator evaluations, confirming the reliability and consistency of the adopted workflow and resulting geological model.

Acknowledgements

This work was supported by the Basra Oil Company (BOC), Basra, Iraq, which provided the essential subsurface data used in this study. The authors gratefully acknowledge the technical assistance from the company and data access that made this research possible.

Credit Authorship Contribution Statement

Abdulrahman N. Al-Ansari: Conceptualization, Data curation, Methodology, Software, Validation, Formal analysis, Visualization, Writing – original draft, Writing – review & editing. Ayad A. Abdulrazaq: Supervision & Validation. Dahlia A. Al-Obaidi: Supervision, Writing – review & editing, Validation.

Declaration of Competing Interest

The authors declare that they have no known competing financial interests or personal relationships that could have appeared to influence the work reported in this paper.

REFERENCES

Al-Dujaili, A.N., Shabani, M. and AL-Jawad, M.S., 2023. Effect of heterogeneity on recovery factor for carbonate reservoirs. A case study for Mishrif Formation in West Qurna Oilfield, Southern Iraq. Iraqi *Journal of Chemical and Petroleum Engineering,* 24(3), pp. 103-111. https://doi.org/10.31699/IJCPE.2023.3.10.

Akinbode, O.B., and Samuel, O.T., 2025. Analysis of an unsupervised clustering algorithm for lithofacies classification in "Riga" field, Niger Delta. *Scientific Research Journal*, 13(4), pp. 19–31. https://doi.org/10.31364/SCIRJ/v13.i04.2025.P04251018.

Al-Ameri, T., Al-Khafaji, A., and Jasim, S., 2015. IRP11 – Yamama Formation oil source assessment using biomarkers & carbon isotope analysis, Ratawi Oil Field, Southern Iraq. *European Association of Geoscientists & Engineers*, 2015, pp. 1 – 5. https://doi.org/10.3997/2214-4609.201414384.

Alhakeem, N.S.A., 2019. Petrophysical study and geological modeling of Yamama Formation in Subba, Luhais, and Ratawi oil fields, Southern Iraq. PhD thesis, University of Baghdad.

Alhakeem, N.S., Nasser, M.E., and Al-Sharaa, G.H., 2019. 3D geological modeling for Yamama reservoir in Subba, Luhais, and Ratawi oil fields, south of Iraq. *Iraqi Journal of Science,* 60(5), pp. 1023–1036. https://doi.org/10.24996/ijs.2019.60.5.12.

Al-Iessa, I.A.A., 2012. Facies reservoir evaluation of Yamama Formation in Ratawi Field, South of Iraq. MSc thesis, University of Basrah.

Al-Iessa, I.A., and Zhang, W.Z., 2023. The methods of determination of stratigraphic boundaries and reservoir units for the Yamama Formation in the Ratawi Oil Field, Southern Iraq. *Iraqi Geological Journal,* 56(1), pp. 285–309. https://doi.org/10.46717/igj.56.1D.21ms-2023-4-30.

Al-Shahwan, M.F., 2002. Thermal maturity nomenclature of the Lower Chalk Sequence, Southern Iraq: Applications for calculating oil potential. PhD thesis, University of Baghdad.

Al-Shahwan, M.F., and Al-Iessa, I.A., 2015. Petrophysical characteristics study of carbonate Yamama reservoir in Ratawi Oil Field, South of Iraq. *Journal of Basrah Researches, Sciences,* 40(4)

Al-Siddiki, A.A., 1978. The geology and the hydrocarbon prospects of the Ratawi, Yamama and Sulaiy Formation in Southeastern Iraq. Subsurface section. Southern Petroleum Organization, Iraq.

Al-Siddiki, A.A., 1977. Subsurface geology of southeastern Iraq. *paper presented at the 10th Arab Petroleum Congress, Tripoli, Libya,* paper no. 141(B-3), P. 47.

Alameedy, U., Almomen, A., and Abd, N., 2023. Evaluating machine learning techniques for carbonate formation permeability prediction using well log data. *Iraqi Geological Journal,* 56(1), pp. 175–187. https://doi.org/10.46717/igj.56.1D.14ms-2023-4-23.

Bassiouni, Z., 1994. Theory, measurement, and interpretation of well logs. *Society of Petroleum Engineers.* https://doi.org/10.2118/9781555630560.

Bateman, R.M., 2012. Openhole log analysis and formation evaluation. Society of Petroleum Engineers. https://doi.org/10.2118/9781613991565.

Chatton, M., and Hart, E., 1962. Announcement of a rock unit redefined: Ratawi Formation. OCE, internal report.

Clavier, C., Coates, G., and Dumanoir, J., 1984. Theoretical and experimental bases for the dual-water model for interpretation of shaly sands. *SPE Journal,* 24(2), pp. 153–168. https://doi.org/10.2118/6859-PA.

Cosentino, L., 2001. Integrated reservoir studies. Editions Technip, *Institut français du pétrole publications*.

Darling, T., 2005a. Chapter 1 – Basics. In: T. Darling (ed.), *Well Logging and Formation Evaluation*. Burlington: *Gulf Professional Publishing*, pp. 1–27. https://doi.org/10.1016/B978-075067883-4/50001-2.

Darling, T., 2005b. Chapter 5 – Advanced log interpretation techniques. In: T. Darling (ed.), Well Logging and Formation Evaluation. Burlington: *Gulf Professional Publishing*, pp. 67–102. https://doi.org/10.1016/B978-075067883-4/50005-X.

Dunnington, H.V., 1958. Stratigraphical distribution of oil fields in the Iraq–Iran–Arabia Basin. *Journal of the Institute of Petroleum*, 53, pp. 129–161.

Egbele, E., Ezuka, I., Onyekonwu, M.O., 2005. Net-to-gross ratios: implications in integrated reservoir management studies. *SPE paper*. https://doi.org/10.2523/98808-MS.

Han, T.C., Yan, H., and Fu, L.Y., 2021. A quantitative interpretation of the saturation exponent in Archie's equations. *Petroleum Science*, 18(2), pp. 444–449. https://doi.org/10.1007/s12182-021-00547-0.

Hilchie, D.W., 1982. Applied openhole log interpretation (for geologists and engineers). *Golden, Colorado,* Dev. Pub. Co., 161 pp.

Jassim, S.Z., and Goff, J.C., 2006. Geology of Iraq. Dolin, Prague.

Khamees, L.A., and Abdulrazzaq, F.N., 2024. Evaluation uncertainty in the volume of oil in place in Mishrif Reservoir. *Journal of Chemical and Petroleum Engineering*, 58(2), pp. 243–254. https://doi.org/10.22059/jchpe.2024.373776.1491.

Kumar, K.C.H., 2010. On the application of Simandoux and Indonesian shaly sand resistivity interpretation models in low and high Rw regimes. *8th Biennial International Conference and Exposition on Petroleum Geophysics*, pp. 1–11. https://spgindia.org/2010/071.pdf.

Kurniawan, D., Winardi, S., and Anggara, F., 2021. Linking between sedimentary facies and petrophysical rock type: a case study. *IOP Conference Series: Earth and Environmental Science*, 789, P. 012077. https://doi.org/10.1088/1755-1315/789/1/012077.

Ma, Y.Z., 2019a. Facies and lithofacies classifications from well logs. In: Y.Z. Ma (ed.), *Quantitative Geosciences: Data Analytics, Geostatistics, Reservoir Characterization and Modeling*. Cham: Springer, pp. 231–254. https://doi.org/10.1007/978-3-030-17860-4_10.

Ma, Y.Z., 2019b. Geostatistical estimation methods: Kriging. In: Y.Z. Ma (ed.), *Quantitative Geosciences: Data Analytics, Geostatistics, Reservoir Characterization and Modeling*. Cham: Springer, pp. 373–401. https://doi.org/10.1007/978-3-030-17860-4_16.

Ma, Y.Z., 2019c. Geostatistical variography for geospatial variables. In: Y.Z. Ma (ed.), *Quantitative Geosciences: Data Analytics, Geostatistics, Reservoir Characterization and Modeling*. Cham: Springer, pp. 301–330. https://doi.org/10.1007/978-3-030-17860-4_13.

Ma, Y.Z., 2019d. Hydrocarbon volumetrics estimation. In: Y.Z. Ma (ed.), *Quantitative Geosciences: Data Analytics, Geostatistics, Reservoir Characterization and Modeling*. Cham: Springer, pp. 539–563. https://doi.org/10.1007/978-3-030-17860-4_22.

Ma, Y.Z., 2019e. Introduction to geological and reservoir modeling. In: Y.Z. Ma (ed.), *Quantitative Geosciences: Data Analytics, Geostatistics, Reservoir Characterization and Modeling*. Cham: Springer, pp. 333–349. https://doi.org/10.1007/978-3-030-17860-4_14.

Ma, Y.Z., 2019f. Introduction to model upscaling, validation and history match. In: Y.Z. Ma (ed.), *Quantitative Geosciences: Data Analytics, Geostatistics, Reservoir Characterization and Modeling*. *Cham: Springer*, pp. 565–591. https://doi.org/10.1007/978-3-030-17860-4_23.

Ma, Y.Z., 2019g. Stochastic modeling of continuous geospatial or temporal properties. In: Y.Z. Ma (ed.), *Quantitative Geosciences: Data Analytics, Geostatistics, Reservoir Characterization and Modeling*. *Cham: Springer*, pp. 403–433. https://doi.org/10.1007/978-3-030-17860-4_17.

Motlaq, H.G., 1999. Sequential stratigraphy of Yamama Formation in Al-Siba field. internal report, Oil Exploration Company, Baghdad.

Murtadha, Z.I., 2012. Reservoir evaluation of Yamama Formation, Ratawi Oil Field. MSc thesis, University of Baghdad.

Murtazin, T., Sergey Usmanov, Marat Validov, and Marat Amerkhanov, 2022. The development of automatic system for geological modeling of extra-viscous oil deposits on the example of Tatarstan Republic. *International Petroleum Technology Conference Proceedings*, D032S172R001. https://doi.org/10.2523/IPTC-22175-MS.

Phan, V., 2002. Modeling technique for generating fluvial reservoir descriptions conditioned to seismic data. PhD thesis, Stanford University. https://earthsci.stanford.edu/ERE/pdf/pereports/Phan02.pdf.

Pickett, G.R., 1966. A review of current techniques for determination of water saturation from logs. *Journal of Petroleum Technology*, 18(11), pp. 1425–1433. https://doi.org/10.2118/1446-PA.

Rabanit, P.M.V., 1952. Rock units of Basrah area. BPC, internal report.

Rozarian, A., 1995. Sedimentological and depositional history of the Yamama Formation, Southern Iraq. INOC, internal report.

Sadooni, F., 1993. Stratigraphic sequence, microfacies, and petroleum prospects of the Yamama Formation, Lower Cretaceous, Southern Iraq. *AAPG Bulletin*, 77, pp. 1971–1988. https://doi.org/10.1306/BDFF8F92-1718-11D7-8645000102C1865D.

Salem, H., and Chilingarian, G., 1999. The cementation factor of Archie's equation for shaly sandstone reservoirs. *Journal of Petroleum Science and Engineering*, 23, pp. 83–93. https://doi.org/10.1016/S0920-4105(99)00011-5.

Santos, A., Scanavini, H.F., Pedrini, H., Schiozer, D.J., Munerato, F.P. and Barreto, C.E., 2022. An artificial intelligence method for improving upscaling in complex reservoirs. *Journal of Petroleum Science and Engineering*, *211*, P. 110071.https://doi.org/10.1016/j.petrol.2021.110071.

Schlumberger, 2018. Petrel software user guide, version 2018. Schlumberger, Houston.

Steineke, M., and Bramkamp, R.A., 1952. Mesozoic rocks of eastern Saudi Arabia. *American Association of Petroleum Geologists Bulletin*, 36(5), P. 909.

Tibshirani, R., Walther, G., and Hastie, T., 2001. Estimating the number of clusters in a data set via the gap statistic. *Journal of the Royal Statistical Society: Series B (Statistical Methodology)*, 63(2), pp. 411–423. http://www.jstor.org/stable/2680607.

TotalEnergies, 2021. Subsurface workshop about Ratawi Field Development Plan. internal Ratawi Field development study, Iraq, Basrah.

Turner, A.K., Kessler, H., van der Meulen, M.J., 2021. Introduction to modeling terminology and concepts. In: *Applied Multidimensional Geological Modeling*. Wiley, pp. 1–12. https://doi.org/10.1002/9781119163091.ch1.

Wang, J., Wancheng Z., Hui L. , Tao Q., and Maiyong Z. , 2025. Three-dimensional geological modeling of thin ore body and complex strata based on multi-point geostatistics. *Engineering Geology*, 352, P. 108056. https://doi.org/10.1016/j.enggeo.2025.108056.

Waxman, M.H., and Smits, L.J.M., 1968. Electrical conductivities in oil-bearing shaly sands. *SPE Journal*, 8(2), pp. 107–122. https://doi.org/10.2118/1863-A.

Zhang, Y., 2009. Introduction to geostatistics – course notes. *Colorado School of Mines*.

تقييم عدم تجانس المكمن من خلال التكامل بين النمذجة البتروفيزيائية والجيولوجية: دراسة حالة لمكمن اليمامة، حقل الرطاوي، جنوب العراق

عبدالرحمن نزار الانصاري [1,2*] ، اياد عبدالحليم عبدالرزاق [1] ، داليا عبدالهادي العبيدي [1]

[1] قسم هندسة النفط، كلية الهندسة، جامعة بغداد، بغداد، العراق

[2] شركة نفط البصرة، البصرة، العراق.

الخلاصة

يمثل بناء نموذج مكمني وتقييم الخواص البتروفيزيائية بدقة ركيزة أساسية للإدارة الفعّالة للمكامن، إذ يتيح تقديرًا موثوقًا لمخزون الهيدروكربونات ويدعم التنبؤات عبر المحاكاة العددية. يهدف هذا البحث إلى توصيف مكمن اليمامة الكربوناتي في حقل رطاوي، جنوبي العراق، وبناء نموذج جيولوجي يمهّد لمحاكاة التنبؤات المستقبلية. تم استخدام المجسات السلكية وتحاليل اللباب والتقارير الجيولوجية، لتحديد حجم السجيل والمسامية الفعالة والتشبع المائي. كما أُجري تصنيف للوجوه الصخرية بالتحليل العنقودي لتوضيح التغاير الليثولوجي. وأُنشئ الإطار التركيبي استنادًا إلى خرائط الكنتور والترابط بين الآبار، أعقبه نمذجة ثلاثية الأبعاد للخواص باستخدام تقنيات جيوإحصائية وصياغة نماذج فاريوغرام لكل وجه ونطاق لتعزيز دقة التوزيع. النتائج اكدت مخرجات الدراسات السابقة بأن تكوين اليمامة يتألف من خمس وحدات رأسية، ثلاث حاملة للنفط (YA, YB, YC) ووحدتان حاجزتان (C1, C2), الا ان هذه الدراسة تميزت بتضمينها لكل الابار التي تخترق التكوين بخلاف الدراسات السابقة التي تصمنت ابار محدودة. وقد تميزت الوحدة YB بأفضل الخصائص، فهي تحمل 63% من الكمية المقدّرة للنفط الأصلي في المكمن (1800 مليون برميل)، بما يتماشى مع تقارير المشغل. عمومًا، تتحسن نوعية المكمن باتجاه الشمال الغربي وتنخفض شرقًا، بينما تتسم المنطقة الجنوبية بخصائص متوسطة.

الكلمات المفتاحية: توصيف المكامن، النمذجة الجيولوجية، المكامن الكربوناتية، التحليل الجيوإحصائي، التحليل العنقودي.